Supporting Information

Synergistic Chemisorbing and Electronic Effects for Efficient CO_2 Reduction Using Cysteamine-Functionalized Gold Nanoparticles

Zhijiang Wang[†, *] Kun Sun[†], Caiyun Liang[†], Lina Wu[‡, *], Zhuangzhuang Niu[‡], Jianmin Gao[§, *]

[†]MIIT Key Laboratory of Critical Materials Technology for New Energy Conversion and Storage, School of Chemistry and Chemical Engineering, Harbin Institute of Technology, Harbin 150001, China.

[‡]Molecular Imaging Research Center of Harbin Medical University, TOF-PET/CT/MR center of the Fourth Hospital of Harbin Medical University, Harbin 150001, China.

[§]School of Energy Science and Technology, Harbin Institute of Technology, Harbin 150001, China.

*E-mail: wangzhijiang@hit.edu.cn (Z. Wang); linawuhmu@hotmail.com (L. Wu)；

yagjm@hit.edu.cn (J. Gao)

1. Materials and methods

1.1 Materials

All chemicals, including ethylene glycol (99.8%), $HAuCl_4$ (99.9%), $NaBH_4$ (99.99%), 1-propanethiol (99%), cystemine (98%), hexane (99%), $KHCO_3$ (99.95%), 1,2,3,4-tetrahydronaphthalene (tetralin, 99%), oleylamine (98%), borane *t*-butylamine complex (TBAB, 99%), ethanol (99.8%), were purchased from Sigma-Aldrich, received without further processing. Au foil (99.95% metal basis) was purchased from Alfa Aesar. Carbon black was obtained from Cabot Corporation. Ultrapure water (18.2 MΩ) was produced from a Millipore Autopure system. The electrolyte was made by dissolving $KHCO_3$ (99.95%) in ultrapure water (18.2 MΩ) without further processing.

1.2 Synthesis of CA-Au NPs

9.08 mg cysteamine and 20 mg carbon-black was dissolved in 10 mL ethylene glycol via sonication for 30 min. The mixture was injected into 46.37 mg $HAuCl_4$ and 10 mL ethylene glycol. The mixed solution was then stirred for 1 h at 0 °C before the solution of 105.24 mg $NaBH_4$ with 2 mL ethylene glycol was added to reduce $HAuCl_4$ to Au NPs under vigorous stirring for 30 min at 0 °C. The product was collected via centrifugation (12000 rpm, 3 min), and was washed by ethanol for 5 times. Then, the product was dried overnight in a vacuum-oven.

1.3 Synthesis of PT-Au NPs

PT-Au NPs were synthesized similar with CA-Au NPs except replacing CA as PT.

1.4 Synthesis of ligand-free Au NPs

200 mg $HAuCl_4$ was dissolved in 10 ml of oleylamine and 10 ml of tetralin at a temperature of 4°C under Ar flow. 0.5 mmol TBAB was dissolved in 1 ml of oleylamine and 1 ml tetralin under vigorous magnetic stirring. This solution was then injected into the $HAuCl_4$ solution, followed stirring for 1 h at 45 °C. 40 ml acetone was added to collect Au NPs via centrifugation

(12000 rpm, 5 min). The product was dispersed in 20 ml hexane, precipitated out by adding 40 ml of ethanol and centrifugation, and re-dispersed in hexane.

The synthesized Au NPs were deposited onto Cabot carbon black by sonicating the mixture of Au NPs dispersion in hexane and carbon black. To dry and remove the surfactant, the Au NPs were annealed overnight in a vacuum-oven at 180 °C.

1.5 Characterizations

The crystal structure of the synthesized samples were detected on a Bruker AXS D5000 diffractometer by recording their X-ray diffraction (XRD) patterns. The morphologies of the prepared samples were obtained by transmission electron microscope (TEM) on a Tecnai G2 F30 electron microscope under an accelerating voltage of 300 keV. TEM samples were prepared by dropping a diluted suspension onto amorphous carbon-coated copper grids and drying in the air. X-ray photoelectron spectroscopy (XPS) of samples was measured using a PHI 5700 X-ray photoelectron spectrometer equipped with a monochromatic Al Kα X-ray source. XAS measurements for the samples were carried out using BL14W1 beamline at the Shanghai Synchrotron Radiation Facility (SSRF). ATR-FTIR spectra of the samples were monitored by an Agilent Cary 600 Series FTIR spectrometer, equipped with a multiple-reflection ATR accessory (PIKE Technologies, custom-modified GladiATR). The IR beam was detected by narrow-band mercury cadmium telluride detector cooled to 77 K. The spectra were collected on the Ge ATR crystal. The background was subtracted and a baseline correction was proceeded to eliminate minor fluctuations.

1.6 Preparation of working electrode

5 mg of the powders were mixed with 950 μL ethanol and 50 μL 5 wt% Nafion solution by sonication for 0.5 h to form a homogeneous ink. Subsequently, 5 μL suspension was drop-dried onto a glassy carbon electrode.

1.7 Electrochemical Measurements

All electrochemical experiments were carried out in a three-electrode system using a Autolab Potentiostat. An airtight two-compartment electrochemical cell was separated by an anion exchange membrane with 0.5 M $KHCO_3$ electrolyte (pH 7.2) in each chamber. The electrolyte in the cathodic compartment was stirred magnetically at a rate of 1000 rpm during electrolysis. A piece of platinum wire was used as the counter electrode. All potentials were measured against an Ag/AgCl reference electrode (3.0 M KCl) and converted to the reversible hydrogen electrode (RHE) reference scale using

$$E \text{ (vs RHE)} = E \text{ (vs Ag/AgCl)} + 0.210 + 0.0591 \times \text{pH} \qquad \text{(S1)}$$

Before electrolysis, the electrolyte in the cathodic compartment was bubbled with CO_2 gas for 1 h. A steady supply of CO_2 gas was delivered at a rate of 20.0 sccm. The gas products were sampled into a gas chromatograph (GC, Aglient 7890A) after a continuous electrolysis of 20 min under each potential. The GC analysis was set up to split the gas sample into two aliquots. One aliquot passed a thermal conductivity detector (TCD), and the other was routed through flame ionization detector (FID). ^{1}H NMR was employed to test for possible liquid-phase products. Their concentration was analyzed on Bruker Avance 400 MHz spectrometer. All potentials were *iR*-corrected.

The electrochemically active surface area is determined by Pb UPD experiment. The electrode was immersed in a 0.1 M NaOH solution containing 1 mM $Pb(OAc)_2$ continuously purged with Ar in a two-compartment electrochemical cell. Pt gauze was used as the reference electrode, and Ag/AgCl (3 M KCl) was used as the reference electrode. Cyclic voltammograms from -0.15 to −0.8 V with a scan rate of 50 mV/s were acquired repeatedly. The anodic stripping wave was integrated to calculate the ECSA of CA-Au NPs、PT-Au NPs and naked Au NPs electrodes.

The Faradaic efficiency and partial current of H_2 and CO production ($FE_{H2\ or\ CO}$ and $i_{H2\ or\ CO}$) were calculated from GC chromatogram peak areas where $V_{H2\ or\ CO}$ is volume concentration of H_2 or CO based on the calibration of the GC. The equation is as following.

$$i_{H_2\ or\ CO} = V_{H_2\ or\ CO} \times Q \times \frac{2Fp_0}{RT} \tag{S2}$$

$$FE_{H_2\ or\ CO} = \frac{i_{H_2\ or\ CO}}{i_{total}} \times 100 \tag{S3}$$

$$mass\ \ activity = \frac{FE_{CO} \times i_{total}}{\beta m_{cat}} \tag{S4}$$

where i_{total} is measured current, F is Faradaic constant, p_0 is pressure, T is temperature and R is ideal gas constant, 8.314 J mol K^{-1}, β is Au weight ratio in total carbon-supported NP catalysts, m_{cat} is catalyst weight.

2. Supporting figures

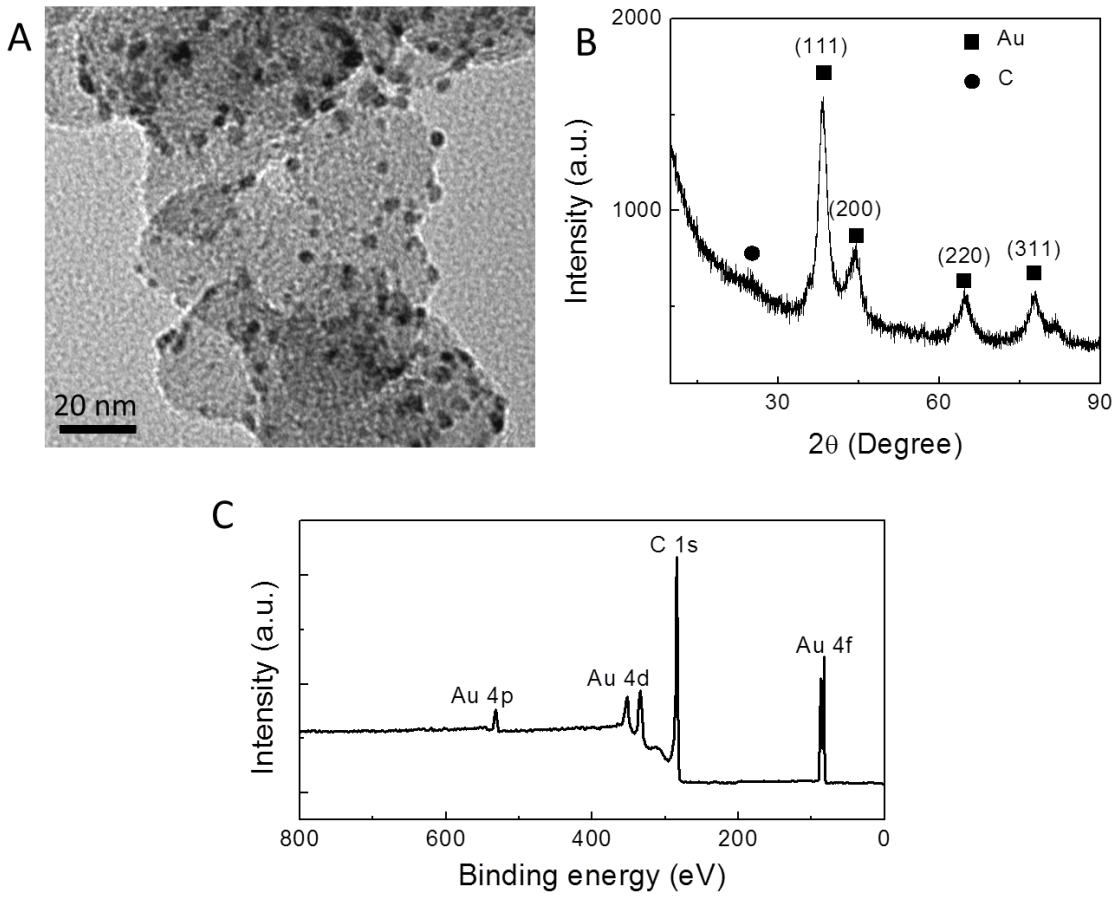

Fig. S1. Characterization on naked Au NPs. (A) TEM image, (B) XRD pattern and (C) XPS analysis. TEM image shows that Au NPs are loaded onto carbon blacks and have particle sizes of around 4.2 nm.

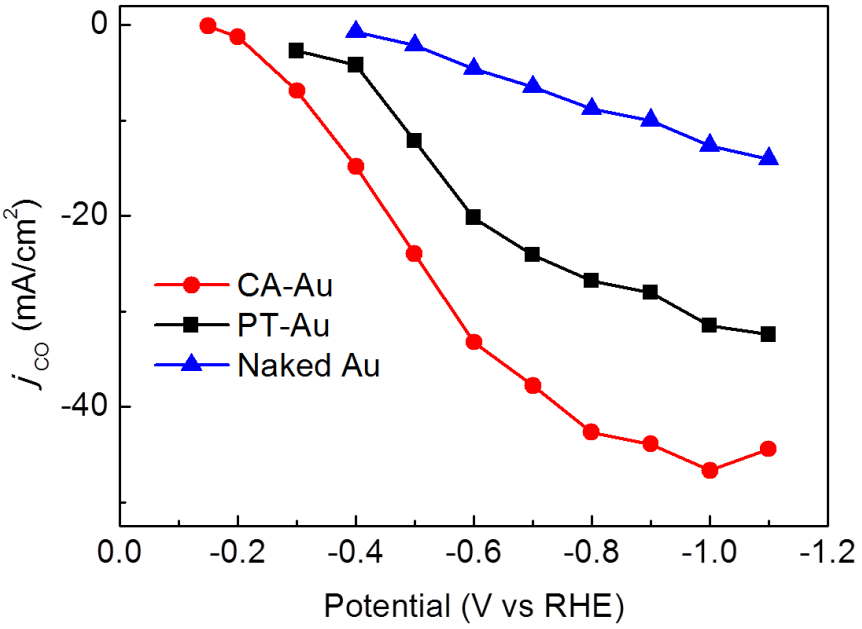

Fig. S2. Current density for CO vs applied potential of three Au-based catalysts for CO_2RR.

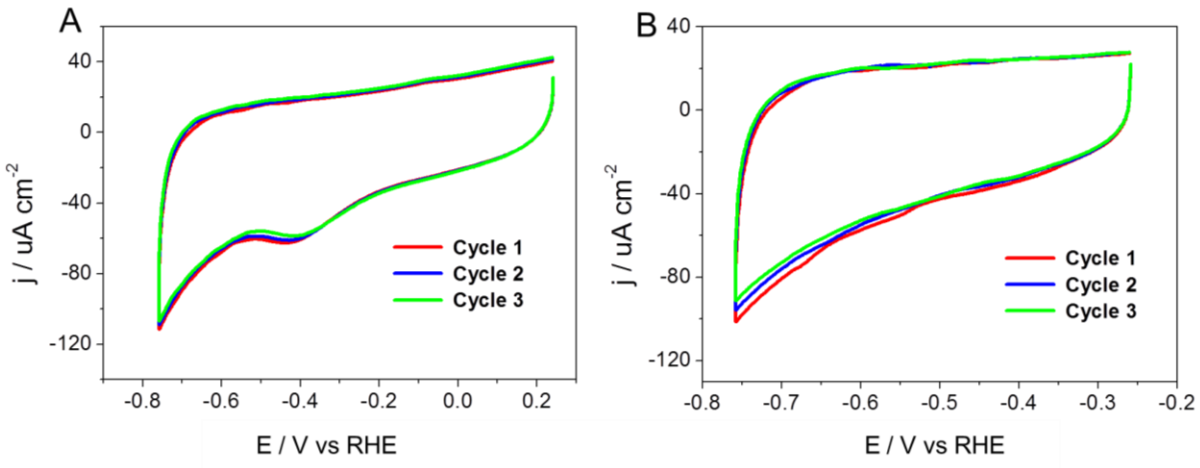

Fig. S3. Cyclic voltammograms for CA-Au NPs with three consecutive scans in 0.5 M $KHCO_3$ solution saturated by CO_2 in potential windows of (+0.2 V ~ -0.8 V) (a) and (-0.3 V ~ -0.8 V) (b). The sweep rate is 0.01 V/s.

Basing on **Fig. S3**, it can be found that the CA- Au NPs keep very high stability. The peak at around -0.4 V vs RHE is caused by cleavage of Au-S bonds. If the alkanethiol ligands have poor stability, the Au-S peak in cyclic voltammogram curves will disappear at the second cathodic scans. For the synthesized CA-Au NPs, the peaks corresponding to Au-S show a little variation under three consecutive scans. When the CV cycling potential range is in -0.8 to -0.3 V, the oxidation of Au-S is depressed. There is no Au-S reduction peak any more. But if the scan potential is extended to -0.8 to 0.2 V, this peak at around -0.4 V will appear again. This gives a strong evidence that the stability of the cysteamine on Au NPs under electrochemical conditions can keep very well.

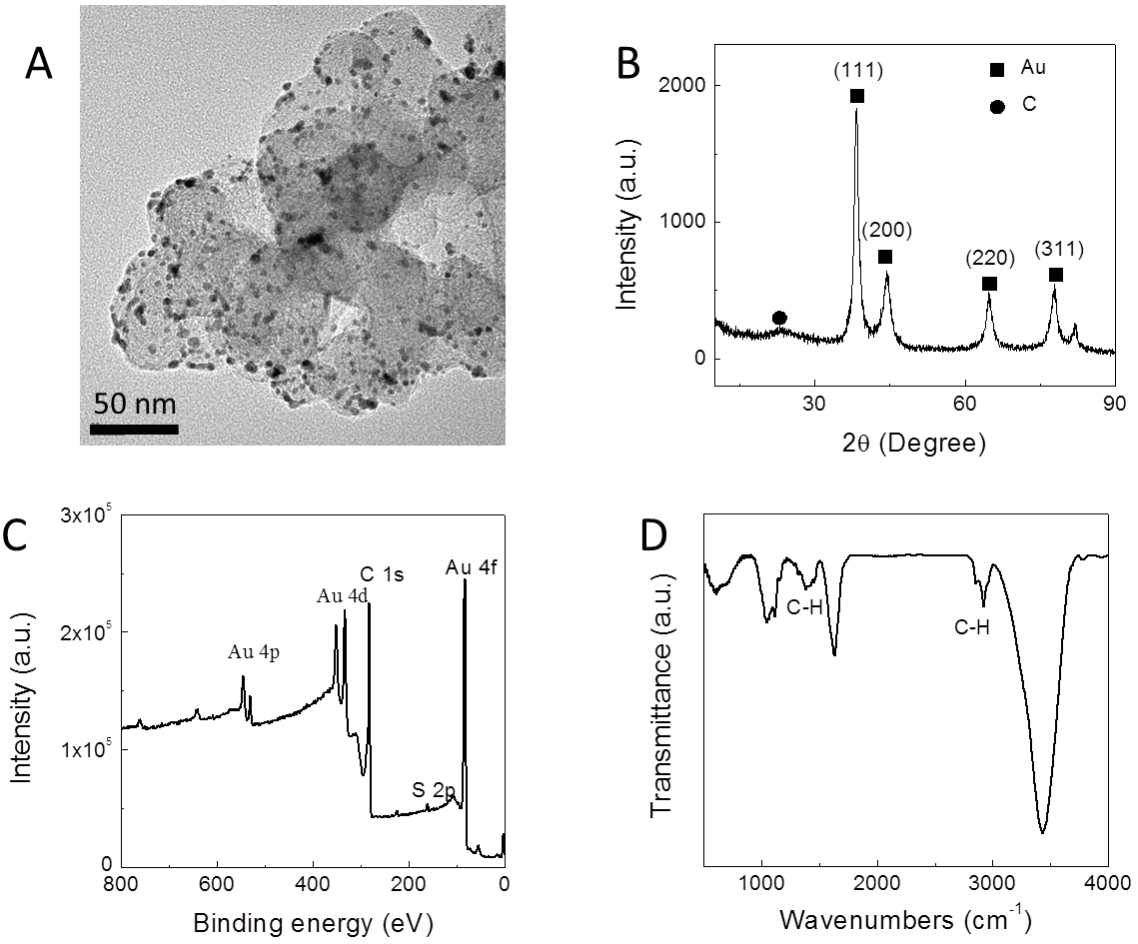

Fig. S4. Characterization on PT-Au NPs. (A) TEM image, (B) XRD pattern, (C) XPS spectrum and (D) FT-IR spectrum. TEM image shows that PT-Au NPs are loaded onto carbon blacks and have particle sizes of around 4.2 nm. XPS and FT-IR spectra indicate the presence of PT molecules on Au NPs.

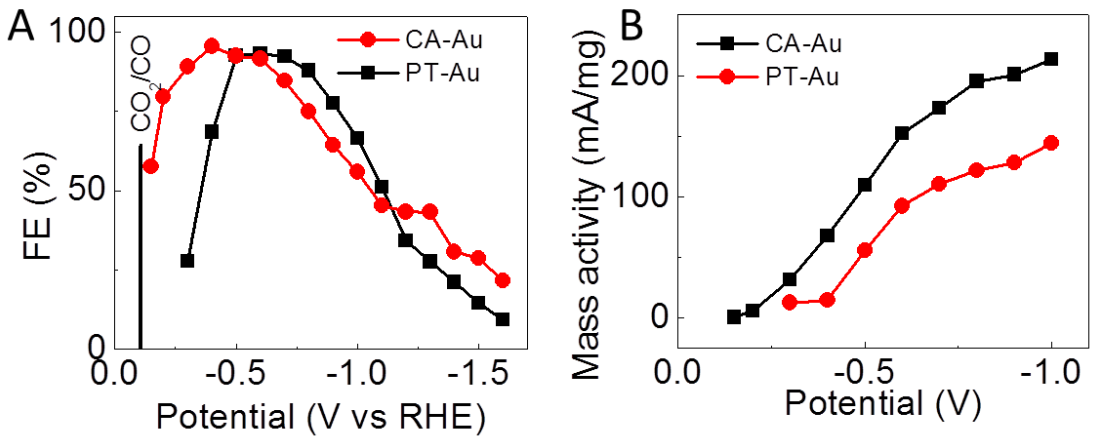

Fig. S5. CO_2RR performance of CA-Au and PT-Au NPs. (A) FE vs potential, (B) partial current densities for CO formation vs potential.

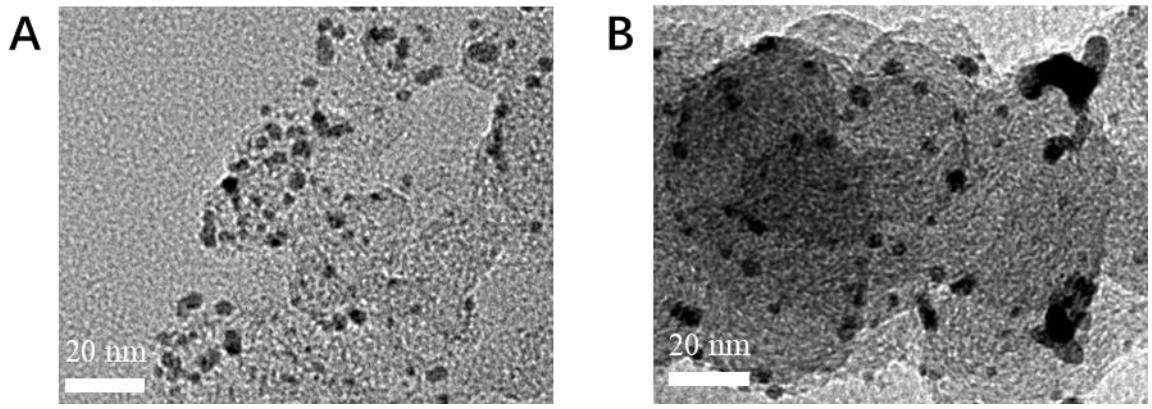

Fig. S6. TEM images of CA-Au and naked Au NPs after 5 hours electrocatalysis. (A) CA-Au NPs, (B) naked Au NPs.

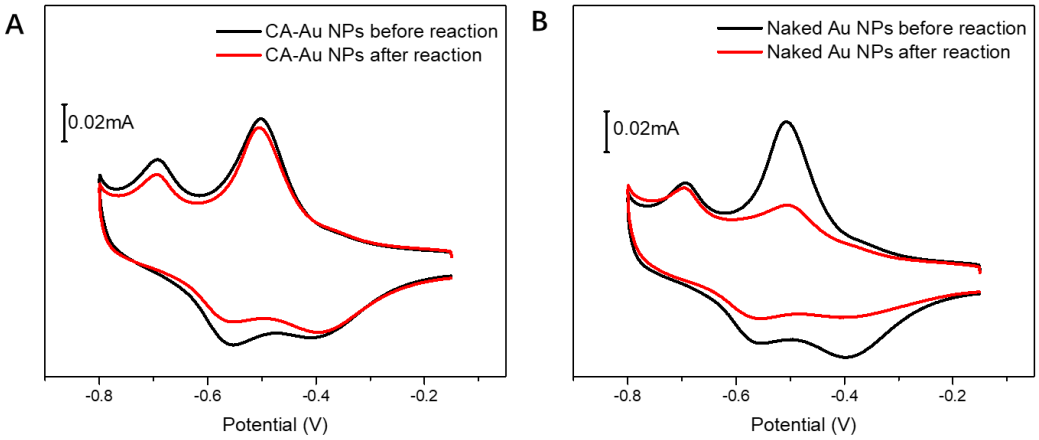

Fig. S7. Pd-UPD profiles of the CA-Au NPs and Naked Au NPs before and after electrocatalysis. (A) CA-Au NPs, (B) naked Au NPs.

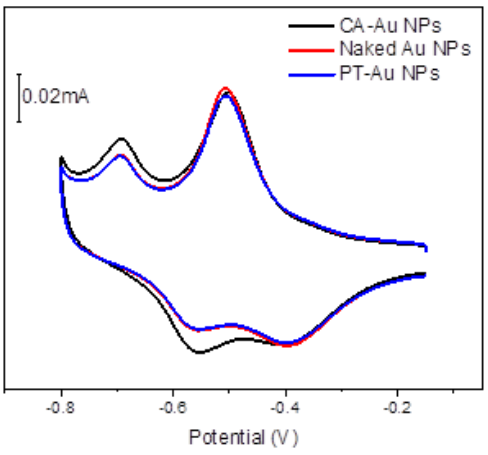

Fig. S8. Pd-UPD profiles of the CA-Au NPs, PT-Au NPs and Naked Au NPs before electrocatalysis.

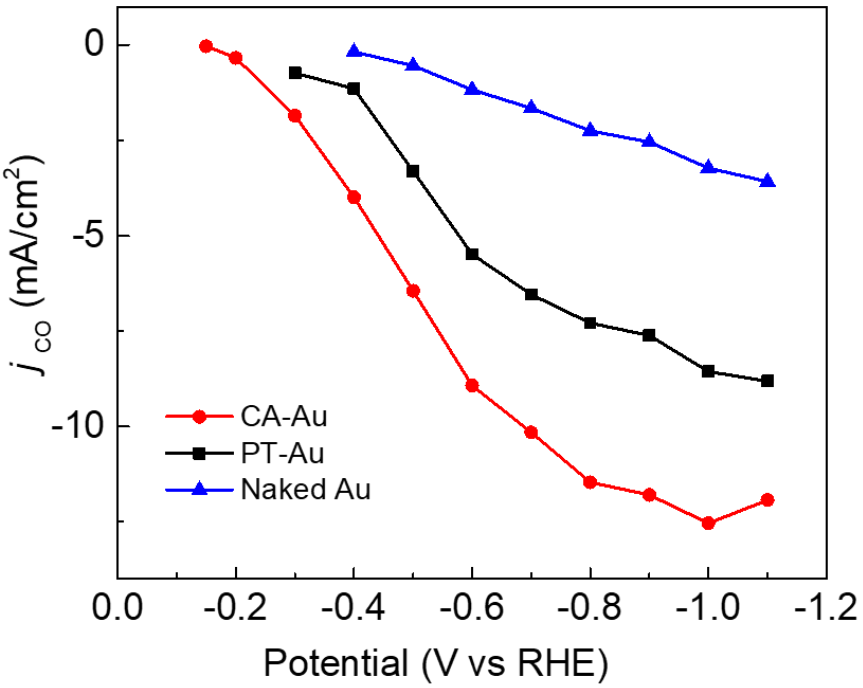

Fig. S9. Area-based CO_2RR activity of the CA-Au NPs, PT-Au NPs and Naked Au NPs.

3. Supporting table

Table S1. Comparison of CO_2 reduction activity for CA-Au NPs with other catalysts. Mass activity was not reported by Refs R4, R6, R9. These noble metal-based nanostructures were prepared on foil. According to the surface feature and reduction activity, their mass activity was comparable to that of nanostructures in R7, but far lower than the value of 3 mA/mg.

Ref	Catalysts	Electrolyte & pH	Onset potential & FE	FE at -0.4V	Mass activity (mA/mg) at -0.4V
This work	CA-Au NPs	0.5M $KHCO_3$ pH 7.2	-0.15 V 57.6%	95.4%	67.9
R1[1]	8 nm Au NPs	0.5M $KHCO_3$ pH 7.2	-0.37 V 22%	35%	0.5
R2[2]	500 nm long Au nanowires	0.5M $KHCO_3$ pH 7.2	-0.2 V 38%	91%	2.8
R3[3]	Au-Fe NPs	0.5M $KHCO_3$ pH 7.2	-0.2 V 80%	97%	48.24
R4[4]	Oxide-derived Au NPs	0.5M $NaHCO_3$ pH 7.2	-0.2 V 10%	96%	N/A
R5[5]	Au Foil	0.5M $KHCO_3$ pH 7.2	-0.4 V 22.6%	22.6%	N/A
R6[6]	Au needles	0.5M $KHCO_3$ pH 7.2	-0.2 V 40%	＞95%	N/A

R7[7]	Nanoporous Ag	0.5M $KHCO_3$ pH 7.2	-0.2 V 3%	89%	0.20 (-0.5 V)
R8[8]	Ag NPs	0.5M $KHCO_3$ pH 7.2	-0.3 V 25%	48%	2.56 (-0.5 V)
R9[9]	Ag nano-corals	0.1M $KHCO_3$ pH 6.8	-0.4 V 76%	73%	N/A

References

1. Zhu, W.; Michalsky, R.; Metin, Ö.; Lv, H.; Guo, S.; Wright, C. J.; Sun, X.; Peterson, A. A.; Sun, S., Monodisperse Au Nanoparticles for Selective Electrocatalytic Reduction of CO2 to CO. J. Am. Chem. Soc. 2013, 135, 16833-16836.
2. Zhu, W.; Zhang, Y.-J.; Zhang, H.; Lv, H.; Li, Q.; Michalsky, R.; Peterson, A. A.; Sun, S., Active and Selective Conversion of CO2 to CO on Ultrathin Au Nanowires. Journal of the American Chemical Society 2014, 136, 16132-16135.
3. Sun, K.; Cheng, T.; Wu, L.; Hu, Y.; Zhou, J.; Maclennan, A.; Jiang, Z.; Gao, Y.; Goddard, W. A.; Wang, Z., Ultrahigh Mass Activity for Carbon Dioxide Reduction Enabled by Gold–Iron Core–Shell Nanoparticles. Journal of the American Chemical Society 2017, 139, 15608-15611.
4. Chen, Y.; Li, C. W.; Kanan, M. W., Aqueous CO2 Reduction at Very Low Overpotential on Oxide-Derived Au Nanoparticles. Journal of the American Chemical Society 2012, 134, 19969-19972.
5. Hori, Y.; Kikuchi, K.; Suzuki, S., Production of CO and CH4 in Electrochemical Reduction of CO2 at Metal Electrodes in Aqueous Hydrogencarbonate Solution. Chem. Lett. 1985, 1695-1698.
6. Liu, M.; Pang, Y.; Zhang, B.; De Luna, P.; Voznyy, O.; Xu, J.; Zheng, X.; Dinh, C. T.; Fan, F.; Cao, C.; de Arquer, F. P. G.; Safaei, T. S.; Mepham, A.; Klinkova, A.; Kumacheva, E.; Filleter, T.; Sinton, D.; Kelley, S. O.; Sargent, E. H., Enhanced electrocatalytic CO2 reduction via field-induced reagent concentration. Nature 2016, 537, 382-386.
7. Lu, Q.; Rosen, J.; Zhou, Y.; Hutchings, G. S.; Kimmel, Y. C.; Chen, J. G.; Jiao, F., A selective and efficient electrocatalyst for carbon dioxide reduction. Nature Communications 2014, 5, 3242.
8. Kim, C.; Jeon, H. S.; Eom, T.; Jee, M. S.; Kim, H.; Friend, C. M.; Min, B. K.; Hwang, Y. J., Achieving Selective and Efficient Electrocatalytic Activity for CO2 Reduction Using Immobilized Silver Nanoparticles. Journal of the American Chemical Society 2015, 137, 13844-13850.
9. Hsieh, Y.-C.; Senanayake, S. D.; Zhang, Y.; Xu, W.; Polyansky, D. E., Effect of Chloride Anions on the Synthesis and Enhanced Catalytic Activity of Silver Nanocoral Electrodes for CO2 Electroreduction. ACS Catalysis 2015, 5, 5349-5356.